# Technical Note: Accurate, reliable and high-resolution air quality predictions by improving the Copernicus Atmosphere Monitoring Service using a novel statistical post-processing method

Angelo Riccio[1,2] and Elena Chianese[1]

[1]Department of Science and Technology, Parthenope University of Naples, Centro Direzionale, Isola C4, 80143, Naples (Italy)
[2]UNESCO Chair on 'Environment, Resources and Sustainable Development', Department of Science and Technology, Parthenope University of Naples, Via F. Petrarca 80, 80123, Naples, Italy

**Correspondence:** Angelo Riccio (angelo.riccio@uniparthenope.it)

**Abstract.** Starting from the regional air quality forecasts produced by the Copernicus Atmosphere Monitoring Service (CAMS), we propose a novel post-processing approach to improve and downscale results on a finer scale. Our approach is based on the combination of Ensemble Model Output Statistics (EMOS) with a spatio-temporal interpolation process performed through the Stochastic Partial Differential Equation-Integrated Nested Laplace Approximation (SPDE-INLA). Our interpolation approach

5  includes several spatial and spatio-temporal predictors, including meteorological variables. A use case is provided that scales down the CAMS forecasts on the Italian peninsula. The calibration is focused on the concentrations of several air quality pollutants ($PM_{10}$, $PM_{2.5}$, $NO_2$ and $O_3$) at daily resolution from a set of 750 monitoring sites, distributed throughout the Italian country. Our results show the key role that conditioning variables play in improving the forecast capabilities of ensemble predictions, thus allowing for a net improvement in the calibration with respect to ordinary EMOS strategies. From a deter-

10  ministic point of view, the performance of the predictive model shows a significant improvement of the performance of the raw ensemble forecast, with an almost zero bias, significantly reduced root mean square errors, and correlations almost always higher than 0.9 for each pollutant; moreover, the post-processing approach is able to significantly improve the prediction of exceedances, even for very low thresholds, such as those recently recommended by the World Health Organisation. This is particularly significant if a forecasting approach is used to predict air quality conditions and plan adequate human health pro-

15  tection measures, even for low alert thresholds. From a probabilistic point of view, the quality of the forecast was verified in terms of reliability and credible intervals. After post-processing, the predictive probability density functions were sharp and much better calibrated than the raw ensemble forecast. Finally, we present some additional results based on a set of gridded (4 km × 4 km) maps covering the entire Italian country, for the detection of areas where pollution peaks occur (exceedances of the current and/or proposed regulatory thresholds).

20  ## 1 Introduction

Outdoor air pollution induced by natural sources and human activities remains a major environmental problem of concern worldwide. Studies have shown that particulate matter, ozone, and nitrogen dioxide degrade ambient air quality and cause

serious health problems to human beings (Kim et al., 2015; Kampa and Castanas, 2008; Manisalidis et al., 2020). For example, recent studies have suggested that air pollution, particularly traffic-related pollution, is associated with preterm birth and infant

25    mortality and the development of asthma and atopy (Khreis et al., 2017; Burbank and Peden, 2018). A joint study of the World Bank and the Institute for Health Metrics and Evaluation (World Bank, 2016) has shown how air pollution also has huge implications for world economies: approximately 5.5 million lives were lost in 2013 from diseases associated with outdoor and indoor air pollution, and with a global economic cost for those deaths of approximately US$225 billion in lost labour income and over US$5 trillion of welfare losses.

30    Producing reliable short-term forecasts of pollutant concentrations is a key challenge in supporting national authorities in their tasks related to EU Air Quality Directives, such as planning and reporting the state of air quality to citizens. Starting in 2014, the Copernicus Atmosphere Monitoring Service (CAMS), a service implemented by the European Centre for Medium-Range Weather Forecasts (ECMWF), continuously provides air quality forecasts throughout Europe, supporting this task. This system is based on an ensemble of several models (Marécal et al., 2015). The different individual model results are interpolated

35    on a common regular $0.1° \times 0.1°$ grid over the European domain (25°W-45°E, 30°N-72°N) for the next four days at an hourly time resolution, and a median ENSEMBLE is calculated from the model output.

Higher spatial resolutions are achieved through smaller-scale applications, such as those used for the FORAIR-IT (Mircea et al., 2014), kAIROS (Stortini et al., 2020), PREV'AIR (Rouil et al., 2009), UK-AIR (DEFRA, 2022) or CALIOPE (Baldasano et al., 2008) systems. However, all these systems require the use of more detailed information and obviously imply the use of

40    much greater computational resources. On the other hand, the use of raw CAMS forecasts do not permit the reproduction of subgrid-scale features, especially close to large point emission sources. There is a reasonable expectation that even the ENSEMBLE results have limited skill under complex local-scale conditions, with expected ensemble mean and variance correlated with the observations and the actual model uncertainty, respectively, and a persistent underestimation of the true observations and model uncertainty.

45    However, understanding how well pollutant concentrations can be predicted in both space and time is essential for a proper assessment of warning and alarm levels and to capture concentration gradients even at high spatial resolutions (Buizza et al., 2022; Chianese et al., 2018; Cohen et al., 2017; Lindström et al., 2014; Zhou et al., 2019). In recent years, there has been an increasing interest in spatio-temporal statistical models, which combine ensemble predictions, data assimilation and machine learning, and these models have quickly gained attention in the air quality scientific community (Bai et al., 2018; Zhang et al.,

50    2012). The reason lies in the fact that hybrid models are easier to implement and do not require high computational resources, while deterministic models are often more computationally expensive and difficult to manage in terms of quality and number of input data requests (Bertrand et al., 2022; Camastra et al., 2022; Chianese et al., 2019; Taheri Shahraiyni and Sodoudi, 2016).

In this study, starting from the CAMS air quality forecasts, we studied the possibility of improving the 24-hour evolution of $PM_{10}$, $PM_{2.5}$ (daily averages), $O_3$ (highest 8-hour daily maximum) and $NO_2$ (1-hour daily maximum) in Italy. This country is

55    characterised by complex conditions for modelling air pollution due to topographic characteristics, different geoclimatic zones, and the complex mix of anthropogenic and natural sources of air pollution. Thus, post-processing of CAMS raw ensemble

results may be particularly suitable for such areas, where the results of the different models could benefit from the use of additional information for a more accurate and higher-resolution estimation.

In this work, a post-processing framework was used to improve the estimation of the air quality forecast in Italy, combining the deterministic forecasts with additional spatio-temporal predictors within a statistical framework. More precisely, we designed an output statistical framework for the output data from CAMS models to obtain a well-calibrated and bias-corrected ensemble prediction and then fit this calibrated ensemble prediction within a spatio-temporal hierarchical model using the integrated Nested Laplace Approximation Stochastic Partial Differential Equation (INLA-SPDE) approach. The INLA-SPDE method is a deterministic approach to Bayesian inference, as opposed to the Markov Chain Monte Carlo (MCMC) method, a simulation-based approach (Gilks et al., 1995; Riccio et al., 2006), for which computational costs are very demanding. Conversely, the INLA-SPDE method has been shown to provide a viable method to speed up calculations, even for large-scale problems, without sacrificing accuracy (Rue et al., 2009).

The remainder of this paper is organised as follows. In Section 2 we first introduce the input data set chosen to analyse pollutant concentrations, and in Section 3 the methods used to develop the post-processing approach. Next, Section 4 discusses results, model validation, and two possible applications of the model estimates for predicting threshold levels in Italy. Conclusions are reported in Section 5.

## 2 Data

### 2.1 The CAMS suite

CAMS provides daily analyses and forecasts of long-range transport of atmospheric pollutants around the world, as well as air quality forecasts for the European domain updated on a daily basis. On a global scale, CAMS provides five-day forecasts for aerosols, atmospheric pollutants, greenhouse gases, as well as stratospheric ozone and UV index. On the European scale, predictions are issued with a resolution of $0.1° \times 0.1°$ over Europe and 10 vertical levels from the Earth surface up to 5000 m, combining data with satellite and non-satellite observations.

The CAMS ensemble prediction system started with a suite composed of seven air quality models: CHIMERE, EMEP, EURAD-IM, LOTOS-EUROS, MATCH, MOCAGE, and SILAM. At the end of 2019, the DEHM (Aarhus University, Denmark) and GEM-AQ (IEP-NRI, Poland) models were added. From June 2022, two additional models (MINNI, operated by ENEA, Italy, and the Barcelona Supercomputing Centre's MONARCH model) deliver their results, as well, expanding the ensemble size to eleven members. The 00:00 UTC ECMWF-IFS (Integrated Forecast System) provides the meteorological data for the prediction of transport phenomena, and the CAMS emission database provides the input data for the simulation of emission phenomena. CAMS forecasts are available for download from the CAMS Atmosphere Data Store. The full range of forecasts is guaranteed to be available by 08:00 UTC every day for the next four days. Marécal et al. (2015) provide the full details on the implementation of this multi-model forecast system.

## 2.2 Training data and predictors

Our ultimate goal is to improve the CAMS forecast on the Italian peninsula. This geographic area is characterised by complex orographic and climatic conditions, including the mountain systems of the Alpine arc (to the north) and Apennines (along the entire longitudinal ridge from north to south), an extensive flat area (the Po valley) and two major islands (Sicily and Sardinia). Furthermore, the transport of desert dust in the Mediterranean region often affects the concentration of PM, with a significant impact on the health of the population (Alahmad et al., 2023; Sajani et al., 2011). This variety of orographic and climatic conditions leads to a high spatial variability of air quality conditions, which makes the Italian peninsula a significant test bed for the predictive capabilities of the CAMS ensemble.

In the present study, the following air quality pollutants have been considered: $PM_{10}$ and $PM_{2.5}$ (daily averages), $O_3$ (highest 8-hour daily maximum), and $NO_2$ (1-hour daily maximum). Table 1 reports the number of ground stations for each of the pollutants measured together with the type of area, the geographic area, and the data coverage (defined as the average percentage of valid data at all monitoring stations for the year 2022). These data are available from the Up-To-Date (UTD) channel of the Air Quality E-reporting system (https://www.eea.europa.eu/data-and-maps/data/aqereporting-9) of the European Environment Agency (EEA), from which they can be freely downloaded.

According to the information communicated to the EEA, the Italian air quality network is made up of a total of 750 monitoring stations, unevenly distributed by area type: most of the monitoring stations are clustered around urban areas, while remote/rural areas are less represented. These monitoring stations are also unevenly distributed with respect to altitude, with most monitoring sites below 250 m. This is not surprising at all, since most of the stations are located where high concentrations are expected, that is, at low-altitude urban or suburban sites. Furthermore, these stations are not evenly distributed with respect to geographic area, with most of the stations located in northern regions and, to a lesser extent, in central and southern Italy.

**Table 1.** Details of observation stations with at least 90% of valid data for the year 2022 grouped by pollutant, geographical area and area type. Data coverage refers to the average percentage of valid data over all monitoring stations.

| Pollutant | Area type | | | Geographical area | | | |
|---|---|---|---|---|---|---|---|
| | rural | suburban | urban | north | centre | south | data coverage |
| $PM_{10}$ | 38 | 59 | 152 | 147 | 59 | 43 | 79% |
| $PM_{2.5}$ | 10 | 29 | 54 | 40 | 31 | 22 | 73% |
| $NO_2$ | 49 | 64 | 189 | 182 | 100 | 20 | 80% |
| $O_3$ | 47 | 39 | 72 | 114 | 37 | 7 | 81% |

As complementary information to the concentration of the main trace pollutants, several geographic and/or meteorological variables may have a potentially predictive role for air quality. The use of spatio-temporal predictors is by no means uncommon in air quality modelling, as they are usually exploited to capture the high-frequency variability at finer spatial scales (Bertrand

et al., 2022; Shtein et al., 2019; Stafoggia et al., 2020). The predictors used in this study can be classified into two different categories: 1) purely spatial predictors, and 2) spatio-temporal predictors. The first category includes all geographic variables that do not have a variable temporal component, while the second category may vary over time. For each monitoring station, we first built a circular buffer with a radius of 5000 m, comparable to the resolution of the raw CAMS predictions, and sampled the density of each purely spatial predictor within this buffer. The purely spatial predictors included in this study are: resident population, imperviousness density, imperviousness built-up, land cover, and road density, re-sampled in two classes (sum of the length of all road segments and sum of the length of main roads (highways and trunks) within the buffer distance). For the spatio-temporal predictors, we took into consideration several meteorological data, all retrieved by the ECMWF operational system and bi-linearly interpolated at each monitoring station location: total daily precipitation, temperature, wind speed and direction, and planetary boundary layer height. For a detailed description of these predictors, see Table A1 in the Supplementary Information section.

These data are expected to show potential predictive capabilities for air quality. For example, temperature, wind speed and direction can cause changes in pollutant concentrations, with higher temperature and wind speed and lower relative humidity favourable for the production of ozone, particulate matter, and nitrogen dioxide (Kayes et al., 2019; Liu et al., 2020; Zhang et al., 2015; Li et al., 2020). The height of the boundary layer is also an important factor in the formation of air pollution, due to enhanced convective activity and scavenging of peroxy radicals (Chen et al., 2019a, b; Levi et al., 2020).
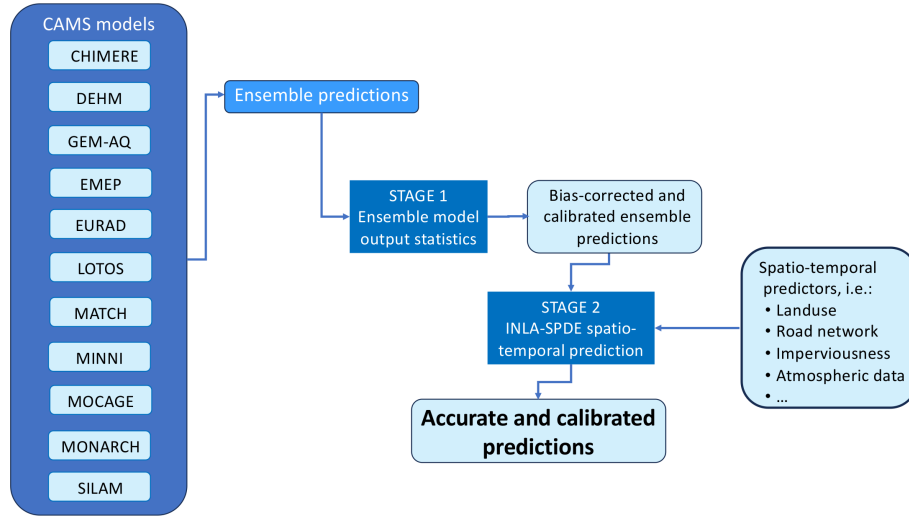
## 3 Methods

### 3.1 The post-processing approach

Ensemble systems are often associated with statistical post-processing steps to inexpensively improve their raw prediction properties (Vannitsem et al., 2021). Starting from raw CAMS data, we propose a two-stage post-processing approach that is capable of removing biases from the output distribution and improving the prediction properties.

A flow chart of the post-processing approach is shown in Figure 1. The first stage is an ensemble model output statistical method (EMOS) (Gneiting et al., 2005), used to obtain a bias-corrected and well-calibrated ensemble. In the second stage, we embed this well-calibrated forecast into a hierarchical spatio-temporal framework, based on the INLA-SPDE method, exploiting the previously listed spatial and temporal predictors.

All statistical analyses have been performed using the combined use of the *R* statistical software, version 4.2.2 (Venables et al., 2022), the Climate Data Operator (CDO), version 2.1.1 (Schulzweida, 2022) and Matlab®, version R2022b Update 3 (MATLAB, 2022), software. Details about these two stages are given in the following two subsections.

### 3.1.1 Stage 1: Calibration of the ensemble

As discussed in Gneiting et al. (2005), the calibration stage has, as the final goal, the maximisation of accuracy subject to reliability. Reliability measures the ability of the ensemble to predict unbiased estimates of the observed frequencies. In short,

**Figure 1.** Flow chart of the post-processing method. The first stage is an Ensemble Model Output Statistical (EMOS) method, based on the output from CAMS models and produces a calibrated and bias-corrected ensemble prediction. The second stage embeds this prediction into the INLA-SPDE spatio-temporal framework, including several spatial and spatio-temporal predictors.

a reliable forecast is one for which there is correspondence between the probability of forecast and the probability of occurrence. Reliability can be measured using the Talagrand histogram (Talagrand and Vautard, 1999; Hamill, 2001) or equivalently the probability integral transform (PIT) histogram (Dawid, 1984; Gneiting et al., 2007). Talagrand and Vautard (1999) fully discuss the properties of the Talagrand and PIT histograms, that is, how their shape can be used to assess when the ensemble results are under/overdispersed.

Reliability is a necessary but not sufficient condition for a valuable ensemble forecast. Another desirable condition is accuracy. An accurate forecast closely resembles the true state of the system; in particular, an ensemble is the more valuable, the greater the accuracy compared to the one obtained with a naive method, such as climatology or persistence.

In the first stage, we applied an EMOS method, 'dressing' the output from the $m$ ensemble member forecasts, $x_1, \ldots, x_m$ using a parametric probability density function (pdf) of the following general form:

$$y|\mu, \sigma^2 \sim f\left(\mu, \sigma^2\right) \tag{1}$$

Here $y$ is the concentration of the chemical pollutant, and $\mu$ and $\sigma^2$ are the expected mean and variance of the pdf, $f$, respectively. The expected mean and variance are estimated from the ensemble member forecasts

$$\begin{cases} \mu = b_0 + b_1 x_1 + \ldots + b_m x_m & \text{(2a)} \\ \sigma^2 = c + dS^2 & \text{(2b)} \end{cases}$$

The equation in (2a) encodes a bias-corrected linear combination, with regression coefficients $b_0, \ldots, b_m$ reflecting the overall performance of any member of the ensemble during the training period relative to the other members. Equation (2b) implements

**6**

the so-called spread-skill relationship (Whitaker and Loughe, 1998), with a non-homogeneous variance that depends linearly on the ensemble variance, $S^2 = \frac{1}{m} \sum_{k=1}^{m} (x_k - x^*)^2$, where $x^* = \frac{1}{m} \sum_{k=1}^{m} x_k$ denotes the ensemble mean. This formulation allows the predictive distribution to exhibit more uncertainty when the ensemble dispersion is large and less uncertainty when the ensemble dispersion is small.

We estimated the coefficients in (2) using a 'global' approach, i.e. a single global calibration was trained on all data using observations from the last $N$ days to predict the concentration for the upcoming day (Bertrand et al., 2022). This process was applied repeatedly every day, mimicking an operational forecasting system, using the previous three days to train the algorithm. With a global approach and with the use of such a short training window, meteorological perturbations on synoptic scales, or changes in emission strengths, can be quickly accounted for through the variation of the parameters estimated during the calibration phase.

We exploited the *crps* (*continuous ranked probability score*) (Gneiting et al., 2007) to optimise coefficient values and applied diagnostic tools, such as the PIT histogram, to evaluate the performance of the calibration stage. The *crps* combines calibration and accuracy in one index, thus allowing the evaluation of predictive performance, based on the paradigm of accuracy maximisation subject to calibration (Gneiting et al., 2007). The full details of this procedure are given in Section B of the supplementary information.

### 3.1.2 Stage 2: Statistical modelling of the space-time process

For a given well-calibrated ensemble prediction, we can exploit additional information that allows higher predictive power (Chang et al., 2020; Singh et al., 2013; Xi et al., 2015). To this aim, we combined the advantages of well-calibrated ensemble results with ancillary predictors, to construct a final spatio-temporally resolved model, which will potentially outperform even the calibrated predictions.

Similarly to other studies (Blangiardo et al., 2013; Cameletti et al., 2013; Fioravanti et al., 2021), for a given calibrated ensemble prediction, $y(t, s_i)$ at time $t$ and spatial location $s_i$, we exploited the following model:

$$y(t, s_i) = \alpha + \mathbf{z}(t, s_i)\boldsymbol{\beta} + \xi(t, s_i) + \epsilon(t, s_i) \tag{3}$$

Here, $\alpha$ represents the overall, space and time constant, average; $\mathbf{z}(t, s_i) = (z_1, \ldots, z_p)$ the vector of $p$ spatio-temporal predictors, each estimated at the same time, $t$, and spatial location, $s_i$, of the calibrated ensemble prediction, and $\boldsymbol{\beta} = (\beta_1, \ldots, \beta_p)$ the corresponding coefficients vector; $\xi(t, s_i)$ encodes for the residual space-time correlation ones the large-scale component $\mathbf{z}(t, s_i)\boldsymbol{\beta}$ is accounted for, and $\epsilon(t, s_i)$ the residual unexplained error, assumed to be generated by a Gaussian white noise process independent over space and time. We used the `r-inla` package (Bakka et al., 2018) to perform all the computations for this second stage. Details of the parameterisation for each component in (3) are given in the Supplementary Information section.

7

## 3.2 Validation

In order to evaluate the improvement in predictive qualities of the results of the first and second stages, we followed a cross-validation approach, splitting the monitoring stations into two data sets: 668 monitoring stations ($\approx 90\%$) were used to train the model in the first stage and then fit the INLA-SPDE model; the remaining 82 ($\approx 10\%$) for validation purposes. Also, note that the INLA-SPDE model includes spatio-temporal correlations among sites (see the $\xi(t, s)$ term in eqn. 3), in order to avoid false confidence in model predictions due to spatial correlations in this cross-validation exercise (Ploton et al., 2020). As already outlined, the monitoring stations are not evenly distributed among the different area type; to mitigate this uneven representativeness issue and improve fairness during the validation stage, the number of urban, suburban and rural stations was selected at random in proportion to their number; precisely, 38 (5.1%) urban, 21 (2.8%) suburban and 23 (3.1%) rural stations were selected for validation purposes and the remaining part was left for training.

A second level of validation was also applied in 'forecasting mode': both the output from the first or second stage can be used to predict the concentration for the next day, i.e. the INLA-corrected values from the second stage can be used to predict the concentrations for the next day, mimicking what could happen when the post-processing phases are applied in a true time forecast mode.

We evaluated the performance of the post-processing stages, using well-known and widely used scoring indices: root mean square error, bias, correlation coefficient, and contingency tables. Furthermore, PIT histograms and credible intervals were used to assess accuracy and reliability.

The contingency tables were built using the thresholds defined by the current Italian legislation (borrowed from the European one) and the new guidelines indicated by the World Health Organisation (WHO), which has reviewed the most recent epidemiological evidence. WHO set stringent and challenging short-term guidelines and interim targets (WHO, 2021); for example, the current threshold value of the Italian legislation for daily $PM_{10}$ concentration is 50 $\mu g/m^3$, 120 $\mu g/m^3$ for the maximum 8-hour daily value for ozone, and 200 $\mu g/m^3$ for the maximum hourly value of $NO_2$. The new WHO air quality guidelines are equal to 45 $\mu g/m^3$ for daily $PM_{10}$, 15 $\mu g/m^3$ for daily $PM_{2.5}$, 100 $\mu g/m^3$ for the maximum 8-hour daily value for $O_3$, and 25 $\mu g/m^3$ for daily $NO_2$ concentration.

## 4 Results

### 4.1 Exploratory analysis

In Appendix B of the Supplementary Information section, we provide an analysis of the skill score of the raw ensemble data, where we take advantage of the same approach described in Murphy (1988), based on the use of a skill score, that is, a measure of the precision of the forecast relative to the precision of the forecast produced by a standard of reference. On average, the root mean square error of the ensemble CAMS predictions is approximately 12 $\mu g/m^3$ for the daily mean $PM_{10}$ concentration, 9 $\mu g/m^3$ for $PM_{2.5}$, 28 $\mu g/m^3$ for the 1-hour $NO_2$ daily maximum and 21 $\mu g/m^3$ for the $O_3$ highest 8-hour daily maximum,

However, as shown in Appendix B, the skill score of all models is systematically worse than that obtained by exploiting a standard of reference (based on the persistence assumption). The median model is only partially able to remedy this condition, usually showing an improvement over the prediction made by the individual models but with a still poor skill score. This points directly to the need, as described in previous sections, to re-calibrate the ensemble and remove the bias.

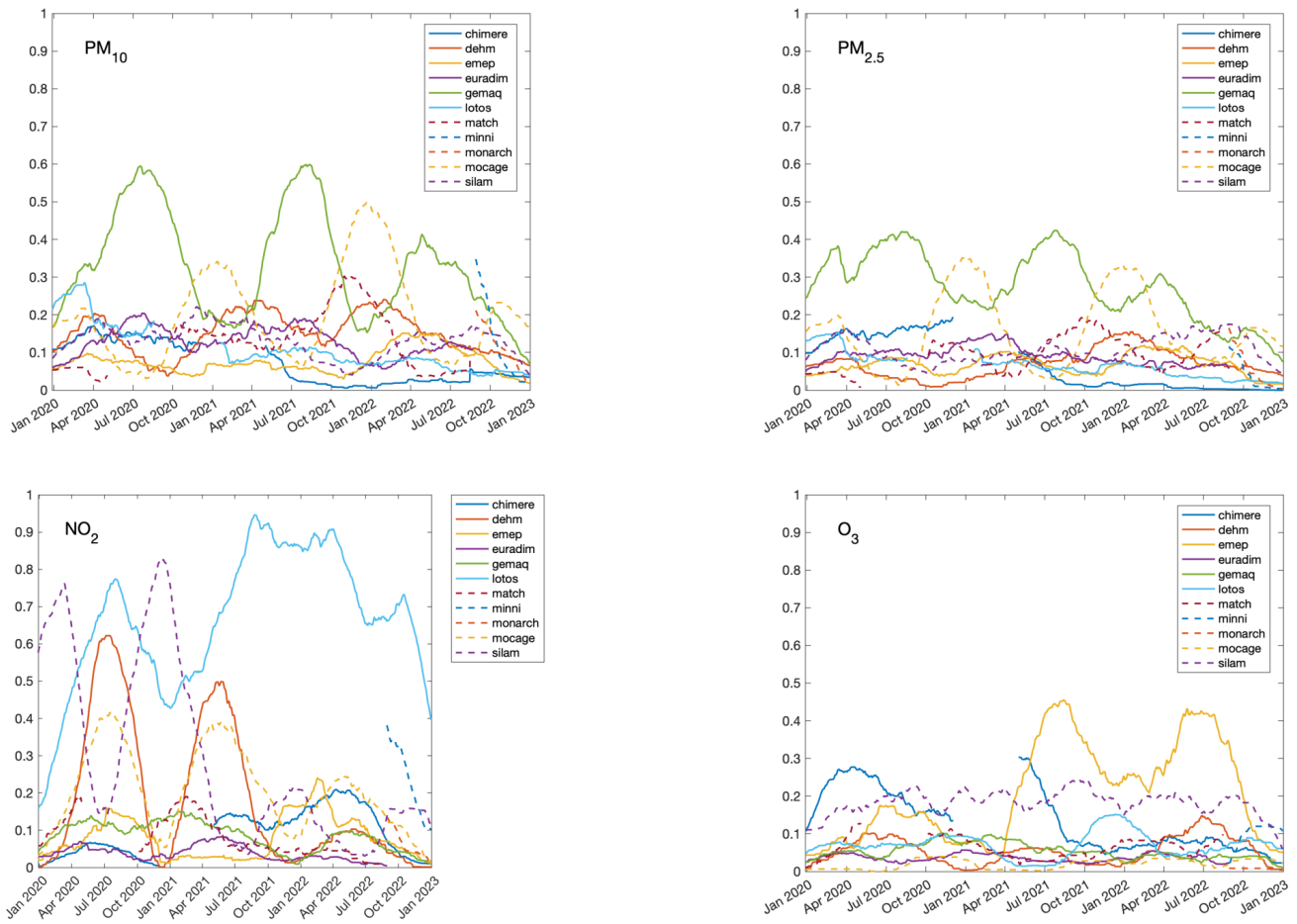## 4.2    The temporal dependence of model weights

Predictions from CAMS are typically constructed by taking the mean value of each cell on the grid to form a single prediction. The use of the ensemble mean with equal weighting has been extensively studied and demonstrated the additional value of the forecast accuracy compared to a single model. In addition, a combination of ensembles can be achieved by assigning weights to different ensembles based on the quality of the forecast. Evidence has shown that by combining models through optimal weights, the multi-model forecasting skill is significantly improved compared to the ensemble predictions of a single model (Raftery et al., 2005; Krishnamurti et al., 2016).

In this work, we also combined forecasts with unequal weights for different members during the first stage to improve accuracy and calibration. The weights themselves can be interpreted as a measure of the relative performance of each individual member compared to the others. To provide a clearer idea of what the temporal dependence of these weights is, Figure 2 shows the weights over an extended period of three years (from 2020 to 2022), using the same procedure described in Section 3.1.1. Weights usually range from 0.05 to 0.3, but a clear seasonal dependence appears for some models. For example, for $PM_{10}$ and $PM_{2.5}$, the GEMAQ and MOCAGE models show a marked seasonal dependence, with the weights of the GEMAQ model increasing significantly during the summer period, while the weights of the MOCAGE model increase during the winter period, indicating their dependence on the season and complementarity. It is also interesting to note that, for ozone, a pollutant with a marked seasonal cycle, most models perform equally well in both the winter and summer seasons.

## 4.3    The added value of the post-processing stages: deterministic-style assessment

### 4.3.1    Root mean square error, bias and correlation

Now we give the results of applying the first and second post-processing stage to the next day predictions for $PM_{10}$, $PM_{2.5}$, $NO_2$ and $O_3$. First, we assessed the performance of the post-processing stages in terms of deterministic scores. Table 2 provides a summary of some of the well-known and widely used scoring measures, that is, root mean square error, bias, and correlation.

The RMSE (root mean square error) and the bias for the training data set for all pollutants were significantly decreased. For example, the RMSE for $PM_{10}$ was reduced by more than half, but the same was also true for all other pollutants. As can be seen, the raw data of the ensemble for $PM_{10}$, $PM_{2.5}$ and $NO_2$ are affected by a negative bias, which is almost zero after the application of the first and second post-processing stage. The high values of the correlation coefficients for the training set (above 0.75 for $PM_{10}$, $PM_{2.5}$ ad $O_3$ after the first stage, and above 0.85 after the second stage) show that the predicted and observed values are well in agreement. Lower scores are obtained for $NO_2$, for which only the exploitation of auxiliary spatio-temporal predictors (in the second stage) is capable of raising its value up to 0.85.

**Figure 2.** Temporal dependence of model weights for $PM_{10}$ (upper-left panel), $PM_{2.5}$ (upper-right panel), $NO_2$ (lower-left panel) and $O_3$ (lower-right panel). To highlight the temporal dependence, the analysis has been extended over three years (from 2020 to 2022, included).

However, it is clear that the results obtained for the training data set are not suitable for a fair comparison. A more reliable estimate of the performance of the post-processing stages can be obtained from the validation data set. These data represent 10% of the measurement stations, randomly selected but stratified according to the type of area in which they are located. The

255   validation data set has not been included in the training process, so the results of the validation data set can be considered as a more reliable and truthful estimate of model performance at different spatial locations. In the case of the validation dataset, we still have a strong reduction of the RMSE and the almost zeroing of the average bias, and a consistent high correlation (usually greater than 0.80), especially after the second stage. The prediction data set refers to the same monitoring stations used for training, but the post-processing framework is used to predict the next day concentrations. As expected, the performances are

260   lower in this case, even if both the first and second stages generally introduce significant improvements both in terms of RMSE, bias, and correlation.

As indicated in Table 1, the measurement stations are unequally distributed with respect to both the type (urban, suburban, or rural) and the geographic location (northern, central, or southern Italy). For example, most measurement stations are located in urban areas, where the concentration of pollutants (especially those of particulate matter and $NO_2$) is higher. Therefore, an

265 interesting perspective on the analysis of the performance of the statistical post-processing process is to verify whether there is a dependence with respect to the type or geographic location, i.e., whether calibrating these stages with a large number of urban stations leads to a consistent bias adjustment across all monitoring stations (regardless of the type or geographic location) or not. To this end, Figure 3 shows the bias for all pollutants for the training data set as a function of the type of monitoring station. The results of the CAMS ensemble tend to underestimate the concentration of particulate matter and $NO_2$, particularly

270 in urban and suburban stations, and overestimate the concentration of ozone (probably related to the underestimation of $NO_2$ in the same areas), although tend to be more successful in rural areas. However, the second stage is able to reduce the bias to almost zero in all types of stations without making a distinction between them.

Figure 4 shows the same results, but reorganised as a function of geographic location. In this case, the second stage is also able to strongly reduce the bias, independently of geographic locations.

275 ### 4.3.2  Sensitivity, specificity and threat score

In order to assess the ability of raw CAMS data, or post-processing models, to predict the exceeding of a given threshold, we built a confusion matrix, categorising each prediction into a true/false positive/negative outcome. The counts from the confusion matrix were used to define the following indices: 1) *sensitivity*, also known as 'true positive rate', defined as the ratio between the number of true positives to the total number of observed exceedances; 2) *specificity*, also known as 'true negative rate',

280 defined as the ratio between true negatives to the total number of observations not exceeding a given threshold; 3) *threat score*, also known as 'critical success index' or 'Jaccard index', defined as the ratio between the number of true positives to the total number of predicted or observed exceedances.

We can consider sensitivity as a measure of how well our predictions can correctly identify exceedances and specificity as a measure of how well our predictions can correctly identify when observations fall short of a given threshold, while the threat

285 score can be seen as a measure of the overlap between the distribution of observations versus that of predictions. A perfect forecast would take a value of 1 for all of these indices.

The sensitivity, specificity, and threat score indexes are plotted in Figure 5 for the validation dataset, where the number of exceedances was defined with respect to the threshold from the new WHO guidelines. The same scores are reported in Figure (E1) of the Supplementary Information section.

290 For $PM_{10}$ and $NO_2$, raw CAMS data show a low precision ($\approx 0.4$), which is greatly improved after the first and second post-processing stages, achieving a value as high as (or even higher than) 0.8. This means that most events above the threshold are missed from the raw CAMS data, but almost always as expected after post-processing stages.

The increase in sensitivity is not accompanied by a decrease in specificity; in most cases, on the contrary, post-processing increases specificity, that is, the number of events correctly classified as below the threshold. The only exception is represented

295 by $NO_2$, for which the specificity decreases after the post-processing stages. However, it should also be said that 25 $\mu$g/m$^3$

**11**
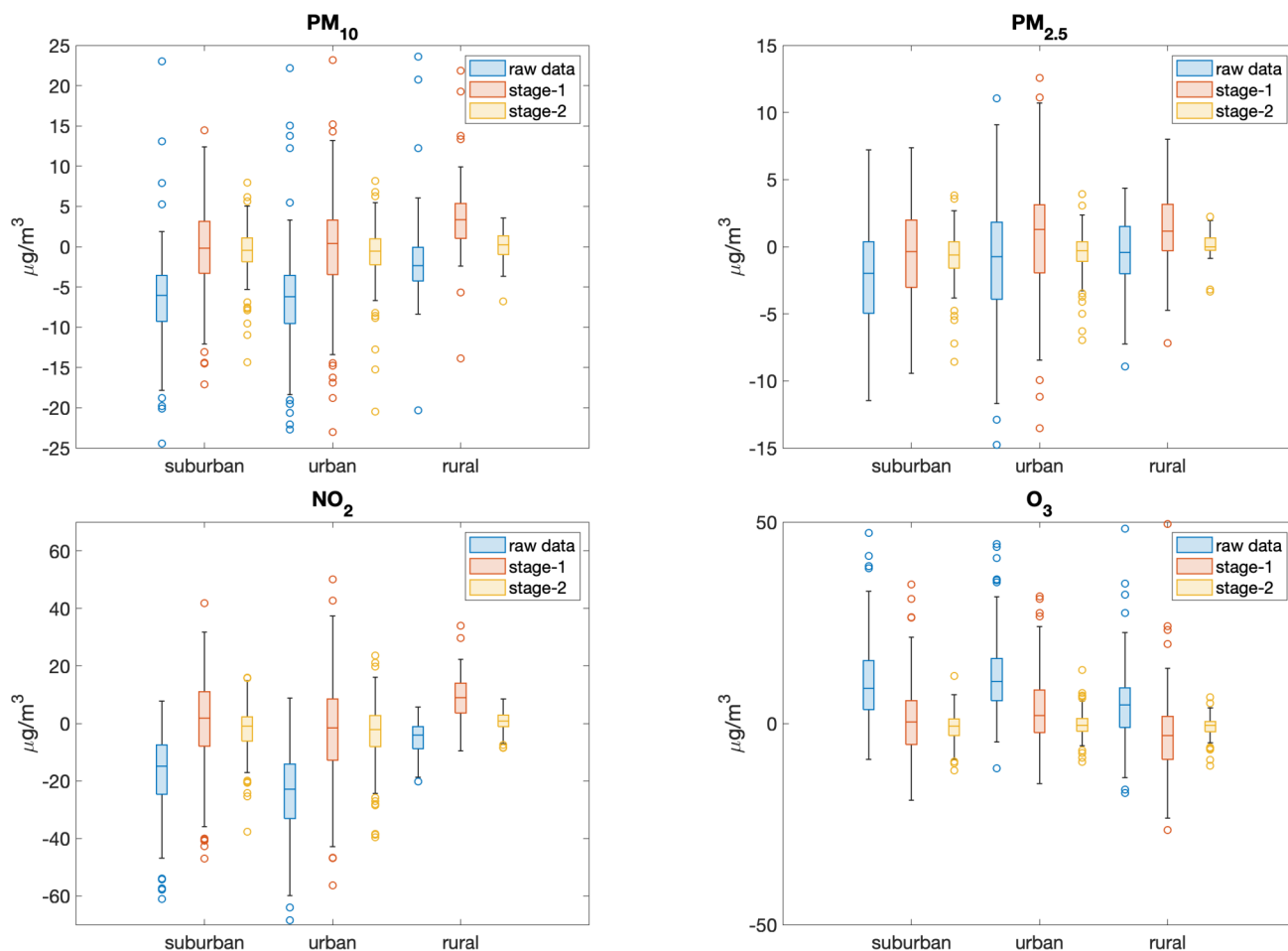
**Figure 3.** Boxplots for the bias for $PM_{10}$ (upper-left panel), $PM_{2.5}$ (upper-right panel), $NO_2$ (lower-left panel) and $O_3$ (lower-right panel), distinguished between the type of monitoring station, for the validation dataset. The light blue boxes correspond to the raw results of the CAMS ensemble, whereas the results after the application of the first and second stages are reported as coral and yellow boxes, respectively.

represents a very low threshold for the 1-hour daily maximum, therefore a low specificity in the capture of events at such low concentrations is expected.

### 4.4 The added value of the post-processing stages: probabilistic-style assessment

RMSE, bias and correlation look for a matching between observations and training/validation/prediction dataset in a 'stiff' mode. However, both the first and the second post-processing stages tailor a statistical 'dress' around results, so that we can use probabilities in measuring the properties of our approach.
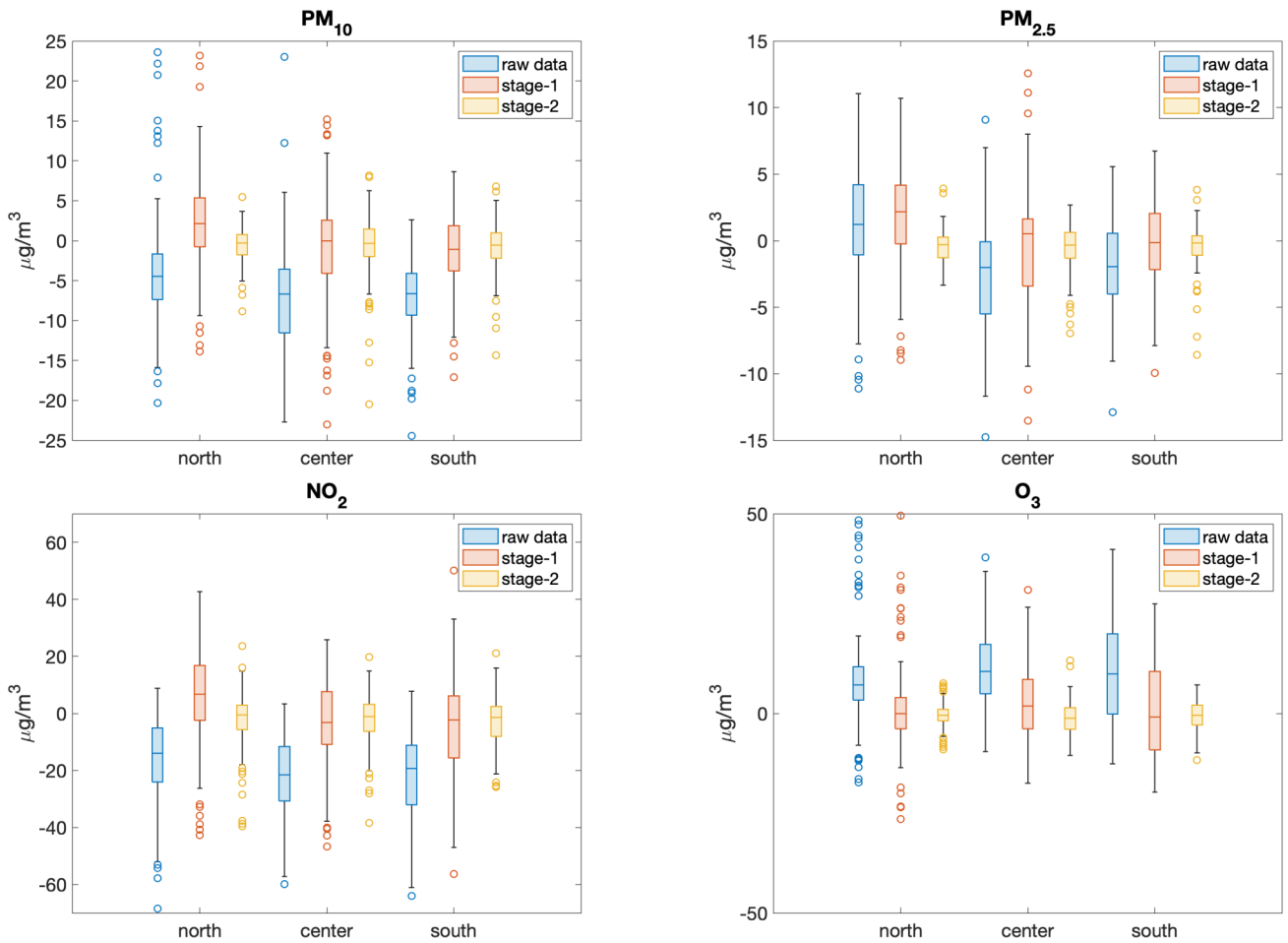
**Figure 4.** Boxplots for the bias for PM$_{10}$ (upper-left panel), PM$_{2.5}$ (upper-right panel), NO$_2$ (lower-left panel) and O$_3$ (lower-right panel), distinguished between the geographic location of monitoring station, for the validation dataset. The light blue boxes correspond to the raw results of the CAMS ensemble, whereas the results after the application of the first and second stage are reported as coral and yellow boxes, respectively.

### 4.4.1 Reliability and accuracy

First, we checked whether our approach ensures reliability while maintaining high accuracy. In a meteorological context, reliability measures the ability of unbiased predictions to closely follow observed frequencies, that is, for a perfectly reliable forecast, an event declared to occur with frequency $p$ is actually predicted with a proportion $p$ on average (Taylor, 2001). Instead, accuracy refers to the degree to which the prediction is close to the observed data. Both are concerned with the conditional probability of predicting an observation for a given forecast. An in-depth discussion of these and other attributes of probabilistic forecasts can be found in Jolliffe and Stephenson (2011).

13
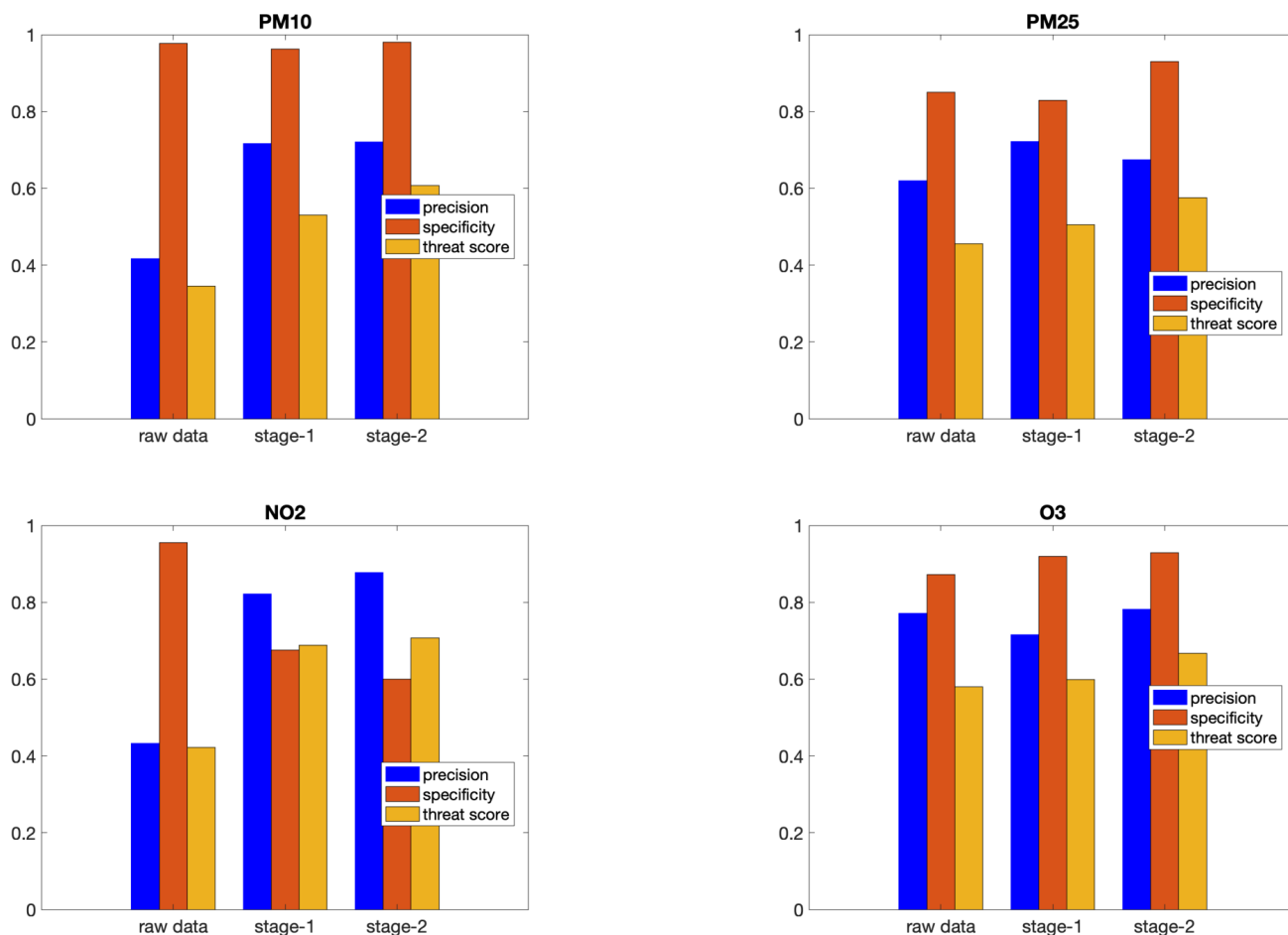
**Figure 5.** Scores (sensitivity, specificity and threat score) for the validation dataset for $PM_{10}$ (upper-left panel), $PM_{2.5}$ (upper-right panel), $NO_2$ (lower-left panel) and $O_3$ (lower-right panel). The blue bars correspond to the raw CAMS results, while the results after the application of the first and second stage are reported as orange and yellow bars, respectively. The number of exceedances (both for observations and predictions) is defined with respect to the new WHO guidelines: 45 $\mu g/m^3$ for daily $PM_{10}$, 15 $\mu g/m^3$ for daily $PM_{2.5}$, 100 $\mu g/m^3$ for the maximum 8-hour daily value for $O_3$, and 25 $\mu g/m^3$ for daily $NO_2$ concentration.

Gneiting et al. (2005), in their seminal work, stated that the goal of a well-calibrated probabilistic forecast is to maximise accuracy, subject to reliability. Figure 6 shows the probability integral transform (PIT) for the raw CAMS predictions and after the application of the first and second post-processing stage to the validation data set. Figure E2 shows the same results in the Supplementary Information, but for the prediction data set. As can be seen, the PIT histograms for the raw CAMS results for $PM_{10}$ and $NO_2$ follow a quasi-monotonic decreasing trend, meaning that the raw CAMS results tend to underestimate observations, while the PIT histogram for $O_3$ shows an inverted-U shape profile, meaning overdispersive behaviour, that is, unnecessarily wide prediction intervals that have higher than nominal coverage. Conversely, the histograms for the validation and
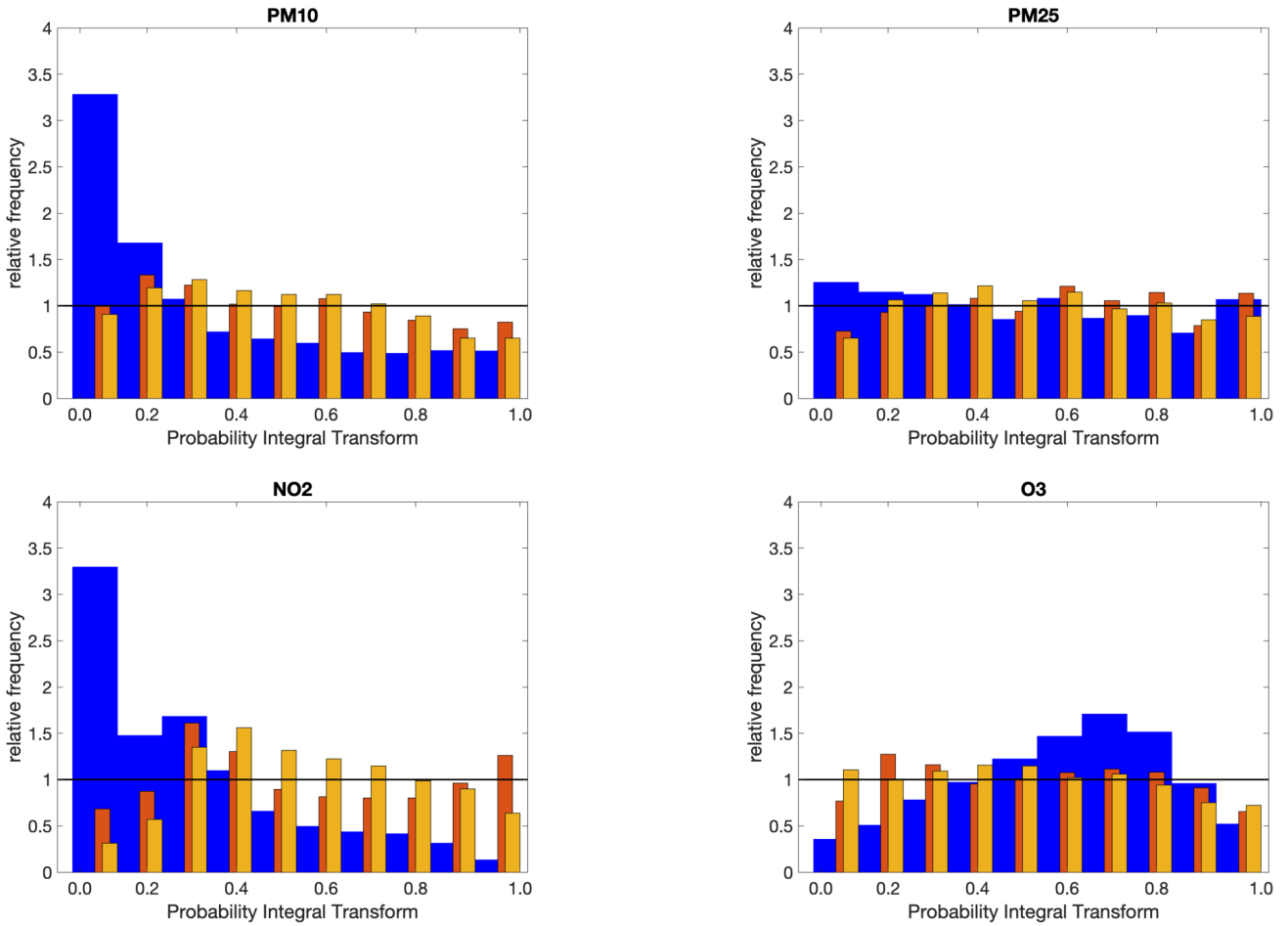
**Figure 6.** PIT for $PM_{10}$ (upper-left panel), $PM_{2.5}$ (upper-right panel), $NO_2$ (lower-left panel) and $O_3$ (lower-right panel). The blue bars correspond to the raw CAMS results, while the results after the application of the first and second stage to the validation dataset are reported as orange and yellow bars, respectively. The orange and yellow bars have been slightly shifted and resized in width so as not to completely overlap the blue bars. The black horizontal lines have been drawn for reference: for a perfect reliable ensemble, the PIT should be flat, with a relative frequency equal to 1.

prediction dataset, after applying the first and second stages, are closer to a flat profile, showing a more accurate reproduction of the probabilities of occurrence, tending to mitigate both the overall bias and over/under-dispersion effects.

### 4.4.2 Credible intervals

The construction of credible intervals from the cumulative distribution function (cdf) is straightforward. For example, the 25th and 75th percentiles of cdf form the lower and upper endpoints of the 50% central prediction interval, respectively, from which

the sharpness, that is, the spread around the predicted value, can be evaluated. For a well-calibrated ensemble, the higher the accuracy, the more data is concentrated around the predicted value, the more value the model adds.

We estimate the 25th and 75th percentiles from the posterior distributions of the first and second stages for each pollutant and compared these results with the interval from the 25th to the 75th percentile from the raw CAMS ensemble data. Table 3 shows the average widths of the 50% probability interval for the raw CAMS data and after the application of the first and second post-processing stage. As can be observed in this table, after the application of the first stage, the credibility interval tends to widen, i.e., the calibrated data show a much smaller bias (see Table 2) but at the cost of widening the credibility interval, making the prediction less accurate. On the other hand, the effect of applying the second stage, through the exploitation of spatial and spatio-temporal predictors, is not only to improve the accuracy of the forecast but also to make the forecast sharper, narrowing the credibility interval. This range is also generally smaller than that obtained from the raw CAMS data. For example, the credibility interval for all pollutants is roughly halved for the validation dataset, going from 8.3 to 4.4 $\mu$g/m$^3$ for PM$_{10}$, from 8.3 to 4.4 $\mu$g/m$^3$ for PM$_{10}$, from 5.3 to 3.3 $\mu$g/m$^3$ for PM$_{2.5}$, from 17.9 to 10.8 $\mu$g/m$^3$ for NO$_2$, and from 13.5 to 15.1 $\mu$g/m$^3$ for O$_3$.

### 4.5 Example of applications

Finally, we want to conclude this section with two examples of potential applications of our post-processing analysis, i.e., (a) interpolation at high spatial resolution and (b) detection of non-compliant areas.

Interpolating data that have been processed in locations not directly observed must consider the issues that come with space-time inhomogeneities and seasonal dependencies. For example, PM$_{10}$/PM$_{2.5}$ are known to be higher during the winter period, especially for urban stations. On the contrary, concentrations in remote stations are relatively low, with a seasonal cycle that favours higher concentrations during the summer season. This is a well-known phenomenon, linked to the activation of convective processes that transport particles emitted at low levels to higher altitudes during the summer period; conversely, urban areas are affected by higher concentrations of particulate matter during the winter period, due to condensation phenomena at low temperatures and atmospheric subsidence (Marinoni et al., 2008). It is also known that NO$_2$ is a short-lived gas in the atmosphere with a lifetime of several hours, especially in the boundary layer during the daytime (Beirle et al., 2011; Lu et al., 2015). Since NO$_x$ emission sources are generally clustered near densely populated urban areas, strong spatial gradients in geographical distribution can be observed from space (Crippa et al., 2018). The relatively low spatial resolution of the CAMS data cannot resolve these steep spatial gradients, and simply merging the results (using equal or unequal weights) into a median prediction cannot remedy this issue.

As shown in Sections 4.3 and 4.4, the forecasts of the raw CAMS data set show significant biases for all pollutants; for example, the raw CAMS data, even when the mean of the ensemble is considered, cannot follow the seasonal cycle for PM$_{10}$, especially for urban stations where the peaks can be higher than 60 $\mu$g/m$^3$. In contrast, statistical post-treatment is capable of rapidly adapting the forecast to the synoptic evolution and removing bias, independently of the type and density of monitoring stations. These properties are also retained when analysing data for the validation dataset, that is, for those stations not directly involved in the training phase. It is reasonable to expect similar performance in unmonitored areas, as, for example, in areas

16

corresponding to a regular grid. To this aim, the calibrated ensemble average from stage 1 was interpolated onto a $4 \times 4$ km regular grid (using a bi-linear interpolation), and the post-processing from stage 2 was applied, using the spatio-temporal predictors estimated at the cell centres of this grid. Figure 7 shows the concentration maps of two exemplary pollutants, $PM_{10}$ and $NO_2$, estimated on the $4 \times 4$ km regular grid for the Italian peninsula.
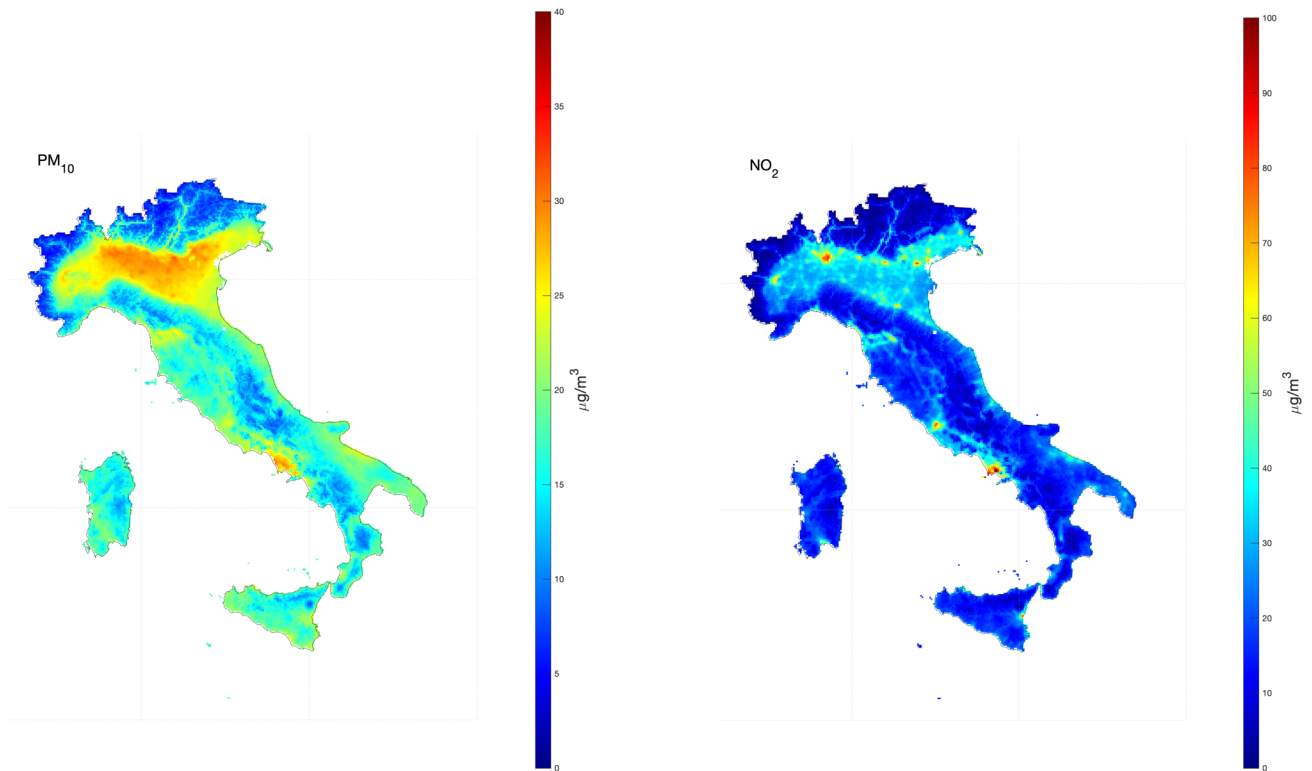


**Figure 7.** Median $PM_{10}$ concentration map (left) of daily means, and median $NO_2$ concentration map (right) of 1-hour daily maximum in 2022, after the application of the second post-processing stage and estimated over a regular $4 \times 4$ km grid resolution.

It is interesting to compare these figures with the median forecast from raw CAMS data. Figures F1 in the Supplementary Information section show the same results, but from the raw CAMS data set. In Figures F1 the pattern is that expected, but it is also clear that the resolution of the CAMS ensemble does not allow one to capture the details on a finer scale, and it obviously does not make much sense to interpolate these data at higher resolutions. Unlike raw CAMS data, the second stage of the statistical post-processing treatment inoculates new information, which allows one to capture finer details, making the space-time interpolation process more realistic and precise (at least for the monitored stations included in the validation process). This applies to both $PM_{10}$ and $NO_2$, where the effects of urban areas and the road network are more evident. Figures G1 show the median values for $PM_{2.5}$ and $O_3$ after post-processing treatment.

A second application concerns the possibility of accurately highlighting the non-compliant areas with a spatial resolution higher than that made available by the CAMS models. WHO recently revised the recommended guidelines to protect the health of the population (WHO, 2021), and in October 2022 the European Commission committed to further improve air quality and align air quality standards with WHO recommendations (EC, 2022). According to the proposal of the European Commission (EC), 'partial alignment' (the so-called policy option I-3) was chosen, because it corresponds to the highest cost-benefit ratio, and the EC recommends the entry into force of this new policy option by 2030, balancing the need for rapid improvements with the need to ensure sufficient response times and coordination with key related policies that will deliver results in 2030 (such as the Fit for 55 package of climate change mitigation policies).

Specifically, in the EC proposal, the new limit values for the protection of human health to be achieved by 2030 are $45 \ \mu g/m^3$ for the $PM_{10}$ daily limit, not to be exceeded more than 18 times per calendar year, and $25 \ \mu g/m^3$ for the $PM_{2.5}$ daily limit, not to be exceeded more than 18 times per calendar year. The post-processing method proposed in this work is ideal for highlighting non-compliant areas, for example using the corrected daily averages for 2022 to detect which areas need to be subject to increased containment measures to meet the 2030 limits.

Figure 8 shows the map of the 95.1st percentile of daily means for $PM_{10}$ and $PM_{2.5}$. The deep red colour marks the areas for which the daily $PM_{10}$ concentration exceeds the threshold of $45 \ \mu g/m^3$ more than 18 times in 2022 (and the threshold of $25 \ \mu g/m^3$ for $PM_{2.5}$). Not surprisingly, large areas with concentrations above the 2030 threshold for $PM_{10}$ are observed in the Po valley and other urban areas (especially the urban area of Naples). Similarly, the $PM_{2.5}$ threshold is particularly challenging to respect. The entire Po valley and the main urban areas (the metropolitan areas of Florence and Naples) all exceed the $PM_{2.5}$ threshold, so strict containment measures will be necessary for a large part of the Italian peninsula.

According to the results of this work, more than 21% of the Italian peninsula exceeds the 2030 threshold for $PM_{2.5}$.

Figures G2 in the Supplementary section show the 95.1st percentile of the highest 8-hour daily maximum for $O_3$ after post-processing treatment. The new EC proposal established a threshold of $120 \ \mu g/m^3$ for this pollutant, but more than 37.3% of the Italian peninsula do not comply with this limit. In this case, not only the Po Valley and the main urban areas are affected by this problem, but also several rural areas and those corresponding to the highest altitudes.

## 5 Conclusions

In this work, the effectiveness of statistical post-processing techniques aimed at improving the accuracy and reliability of the predictions of the air quality models of the CAMS suite have been tested. It is well known that the CAMS suite (currently made up of eleven members), while representing the state-of-the-art of atmospheric modelling, show significant biases, for which it is advisable to adopt post-processing techniques that are statistically reliable and computationally inexpensive to cope with operational constraints. Furthermore, predictions are currently available with moderate spatial resolution ($0.1° \times 0.1°$), and may miss steep spatial gradients that occur in the vicinity of large urban areas and industrial sites.

In order to ameliorate these problems, a statistical post-processing technique was developed and applied to the Italian region, capable of correcting both the bias and the reliability of ensemble predictions. Concentrations of the main air pollutants, $PM_{10}$,

18
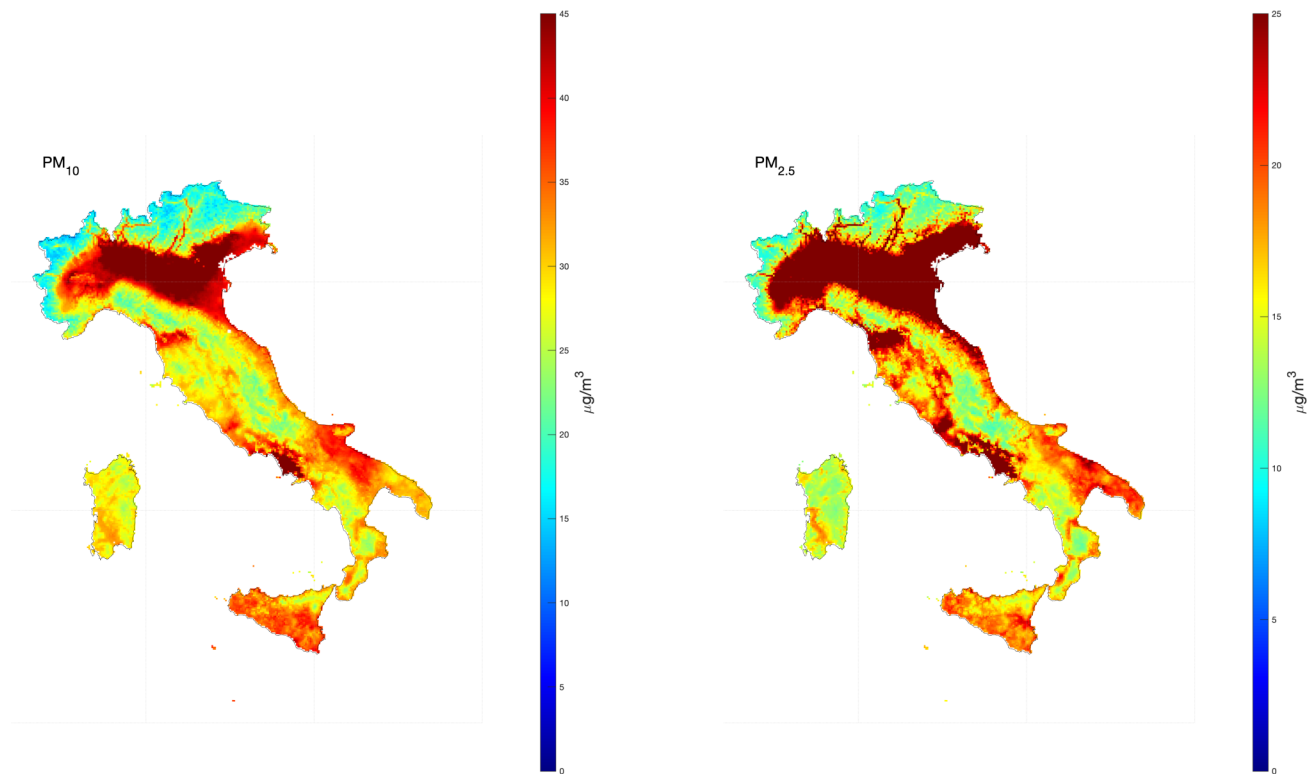
**Figure 8.** 95.1st percentile of $PM_{10}$ (left) and $PM_{2.5}$ (right) after the application of the second post-processing stage and estimated over a regular $4 \times 4$ km grid resolution.

$PM_{2.5}$, $NO_2$ and $O_3$, were taken into account, and a new two-stage post-processing approach was designed, able to meet operational constraints. In the first stage, the ensemble data were combined together through minimisation of the continuous ranked probability score (crps) on the training data. During the second stage, the ensemble prediction was corrected exploiting additional spatio-temporal predictors within a framework based on the INLA-SPDE approach. The post-processing stages make use of a short training period (three days), so as to rapidly adapt to changes in meteorological or emission conditions and apply simultaneously to all monitoring stations.

The post-processing approach is computationally inexpensive. For example, the application of the post-processing method for one day usually costs less than 40 seconds on a typical desktop computer (we used an iMac computer equipped with a 3.4GHz Intel i5 quad-core processor and 16GB 2.4GHz DDR4 memory). This computational time is competitive with respect to other approaches (for example, complex spatio-temporal hierarchical models within a Markov Chain Monte Carlo framework), mainly due to the efficient use of sparse matrices and the Laplace approximation for numerical integration schemes (Bakka et al., 2018).

The validation procedure shows that the post-processing stages were able to remove systematic biases, improve accuracy, and provide reliable forecasts. Moreover, the global approach allowed the application of the INLA-SPDE framework to a regularly spaced grid (with a resolution higher than that of the original CAMS members), highlighting the regions in which

415 exceedances occur.

The post-processing correction process has been applied to the measurement stations for the year 2022 for Italy, but this procedure can be easily generalised to any spatial and temporal region. Because of its flexibility, we also expect that this approach is prone to adapt in real time to fast changes in meteorological conditions and/or abrupt changes in pollutant emissions.

*Code and data availability.* The full list of source codes and dataset used in this work are archived by the authors and can be obtained from

420 the corresponding author upon request

*Sample availability.* The source codes, along with a sample of input files, are available from github, and a local clone can be generated by the command: `git clone https://github.com/angeloriccio/EMOS.git`

*Author contributions.* AR worked on the implementation of the study and performed the simulations with support from EC. EC was responsible for the acquisition of the observed air quality data. AR performed the analysis with the support of EC for results interpretation. AR

425 wrote this article, with contributions from EC.

*Competing interests.* The authors declare that they have no conflict of interest

## References

Alahmad, B., Khraishah, H., Achilleos, S., and Koutrakis, P.: Epidemiology of Dust Effects: Review and Challenges, Dust and Health: Challenges and Solutions, pp. 93–111, 2023.

430   Bai, L., Wang, J., Ma, X., and Lu, H.: Air pollution forecasts: An overview, International Journal of Environmental Research and Public Health, 15, 780, 2018.

Bakka, H., Rue, H., Fuglstad, G.-A., Riebler, A., Bolin, D., Illian, J., Krainski, E., Simpson, D., and Lindgren, F.: Spatial modeling with R-INLA: A review, Wiley Interdisciplinary Reviews: Computational Statistics, 10, e1443, 2018.

Baldasano, J., Jiménez-Guerrero, P., Jorba, O., Pérez, C., López, E., Güereca, P., Martín, F., Vivanco, M., Palomino, I., Querol, X., et al.:

435   Caliope: an operational air quality forecasting system for the Iberian Peninsula, Balearic Islands and Canary Islands–first annual evaluation and ongoing developments, Advances in Science and Research, 2, 89–98, 2008.

Beirle, S., Boersma, K. F., Platt, U., Lawrence, M. G., and Wagner, T.: Megacity Emissions and Lifetimes of Nitrogen Oxides Probed from Space, Science, 333, 1737–1739, 2011.

Bertrand, J.-M., Meleux, F., Ung, A., Descombes, G., and Colette, A.: Improving the European air quality forecast of Copernicus Atmosphere

440   Monitoring Service using machine learning techniques, Atmospheric Chemistry and Physics Discussions, pp. 1–28, 2022.

Blangiardo, M., Cameletti, M., Baio, G., and Rue, H.: Spatial and spatio-temporal models with R-INLA, Spatial and spatio-temporal Epidemiology, 4, 33–49, 2013.

Buizza, C., Casas, C. Q., Nadler, P., Mack, J., Marrone, S., Titus, Z., Le Cornec, C., Heylen, E., Dur, T., Ruiz, L. B., et al.: Data learning: integrating data assimilation and machine learning, Journal of Computational Science, 58, 101 525, 2022.

445   Burbank, A. J. and Peden, D. B.: Assessing the impact of air pollution on childhood asthma morbidity: How, When and What to do, Current Opinion in Allergy and Clinical Immunology, 18, 124, 2018.

Camastra, F., Capone, V., Ciaramella, A., Riccio, A., and Staiano, A.: Prediction of environmental missing data time series by Support Vector Machine Regression and Correlation Dimension estimation, Environmental Modelling & Software, 150, 105 343, 2022.

Cameletti, M., Lindgren, F., Simpson, D., and Rue, H.: Spatio-temporal modeling of particulate matter concentration through the SPDE

450   approach, AStA Advances in Statistical Analysis, 97, 109–131, 2013.

Chang, Y.-S., Abimannan, S., Chiao, H.-T., Lin, C.-Y., and Huang, Y.-P.: An ensemble learning based hybrid model and framework for air pollution forecasting, Environmental Science and Pollution Research, 27, 38 155–38 168, 2020.

Chen, H., Zhuang, B., Liu, J., Wang, T., Li, S., Xie, M., Li, M., Chen, P., and Zhao, M.: Characteristics of ozone and particles in the near-surface atmosphere in the urban area of the Yangtze River Delta, China, Atmospheric Chemistry and Physics, 19, 4153–4175, 2019a.

455   Chen, J., Shen, H., Li, T., Peng, X., Cheng, H., and Ma, C.: Temporal and spatial features of the correlation between $PM_{2.5}$ and $O_3$ concentrations in China, International Journal of Environmental Research and Public Health, 16, 4824, 2019b.

Chianese, E., Galletti, A., Giunta, G., Landi, T., Marcellino, L., Montella, R., and Riccio, A.: Spatiotemporally resolved ambient particulate matter concentration by fusing observational data and ensemble chemical transport model simulations, Ecological Modelling, 385, 173–181, 2018.

460   Chianese, E., Camastra, F., Ciaramella, A., Landi, T. C., Staiano, A., and Riccio, A.: Spatio-temporal learning in predicting ambient particulate matter concentration by multi-layer perceptron, Ecological Informatics, 49, 54–61, 2019.

Cohen, A. J., Brauer, M., Burnett, R., Anderson, H. R., Frostad, J., Estep, K., Balakrishnan, K., Brunekreef, B., Dandona, L., Dandona, R., et al.: Estimates and 25-year trends of the global burden of disease attributable to ambient air pollution: an analysis of data from the Global Burden of Diseases Study 2015, The Lancet, 389, 1907–1918, 2017.

465 Cressie, N. and Wikle, C. K.: Statistics for spatio-temporal data, John Wiley & Sons, 2015.

Crippa, M., Guizzardi, D., Muntean, M., Schaaf, E., Dentener, F., van Aardenne, J. A., Monni, S., Doering, U., Olivier, J. G. J., Pagliari, V., and Janssens-Maenhout, G.: Gridded emissions of air pollutants for the period 1970–2012 within EDGAR v4.3.2, Earth System Science Data, 10, 1987–2013, 2018.

Dawid, A. P.: Present position and potential developments: Some personal views statistical theory the prequential approach, Journal of the

470 Royal Statistical Society: Series A (General), 147, 278–290, 1984.

DEFRA, Department for Environment Food & Rural Affairs: Air pollution forecast map, https://uk-air.defra.gov.uk/forecasting/, last accessed: 2023-05-15, 2022.

EC: Directive of the European Parliament and of the Council on ambient air quality and cleaner air for Europe, https://eur-lex.europa.eu/legal-content/IT/TXT/?uri=CELEX:52022PC0542, last accessed: 2023-09-15, 2022.

475 Fioravanti, G., Martino, S., Cameletti, M., and Cattani, G.: Spatio-temporal modelling of $PM_{10}$ daily concentrations in Italy using the SPDE approach, Atmospheric Environment, 248, 118 192, 2021.

Gilks, W. R., Richardson, S., and Spiegelhalter, D.: Markov chain Monte Carlo in practice, CRC press, 1995.

Gneiting, T., Raftery, A. E., Westveld, A. H., and Goldman, T.: Calibrated probabilistic forecasting using ensemble model output statistics and minimum CRPS estimation, Monthly Weather Review, 133, 1098–1118, 2005.

480 Gneiting, T., Balabdaoui, F., and Raftery, A. E.: Probabilistic forecasts, calibration and sharpness, Journal of the Royal Statistical Society: Series B (Statistical Methodology), 69, 243–268, 2007.

Hamill, T. M.: Interpretation of rank histograms for verifying ensemble forecasts, Monthly Weather Review, 129, 550–560, 2001.

Jolliffe, I. T. and Stephenson, D. B.: Forecast verification: a practitioner's guide in atmospheric science, John Wiley & Sons, Ltd, 2011.

Kampa, M. and Castanas, E.: Human health effects of air pollution, Environmental Pollution, 151, 362–367, 2008.

485 Kayes, I., Shahriar, S. A., Hasan, K., Akhter, M., Kabir, M., and Salam, M.: The relationships between meteorological parameters and air pollutants in an urban environment, Global Journal of Environmental Science and Management, 5, 265–278, 2019.

Khreis, H., Kelly, C., Tate, J., Parslow, R., Lucas, K., and Nieuwenhuijsen, M.: Exposure to traffic-related air pollution and risk of development of childhood asthma: a systematic review and meta-analysis, Environment International, 100, 1–31, 2017.

Kim, K.-H., Kabir, E., and Kabir, S.: A review on the human health impact of airborne particulate matter, Environment International, 74,

490 136–143, 2015.

Konstantinoudis, G., Cameletti, M., Gómez-Rubio, V., Gómez, I. L., Pirani, M., Baio, G., Larrauri, A., Riou, J., Egger, M., Vineis, P., et al.: Regional excess mortality during the 2020 COVID-19 pandemic in five European countries, Nature Communications, 13, 482, 2022.

Krishnamurti, T., Kumar, V., Simon, A., Bhardwaj, A., Ghosh, T., and Ross, R.: A review of multimodel superensemble forecasting for weather, seasonal climate, and hurricanes, Reviews of Geophysics, 54, 336–377, 2016.

495 Levi, Y., Dayan, U., Levy, I., Broday, D. M., et al.: On the association between characteristics of the atmospheric boundary layer and air pollution concentrations, Atmospheric Research, 231, 104 675, 2020.

Li, H., Xu, X.-L., Dai, D.-W., Huang, Z.-Y., Ma, Z., and Guan, Y.-J.: Air pollution and temperature are associated with increased COVID-19 incidence: a time series study, International journal of infectious diseases, 97, 278–282, 2020.

Lindgren, F., Rue, H., and Lindström, J.: An explicit link between Gaussian fields and Gaussian Markov random fields: the stochastic partial
500      differential equation approach, Journal of the Royal Statistical Society: Series B (Statistical Methodology), 73, 423–498, 2011.

Lindström, J., Szpiro, A. A., Sampson, P. D., Oron, A. P., Richards, M., Larson, T. V., and Sheppard, L.: A flexible spatio-temporal model
     for air pollution with spatial and spatio-temporal covariates, Environmental and Ecological Statistics, 21, 411–433, 2014.

Liu, T., Wang, X., Hu, J., Wang, Q., An, J., Gong, K., Sun, J., Li, L., Qin, M., Li, J., et al.: Driving forces of changes in air quality during the
     COVID-19 lockdown period in the Yangtze River Delta Region, China, Environmental Science & Technology Letters, 7, 779–786, 2020.

505 Lu, Z., Streets, D. G., de Foy, B., Lamsal, L. N., Duncan, B. N., and Xing, J.: Emissions of nitrogen oxides from US urban ar-
     eas: estimation from Ozone Monitoring Instrument retrievals for 2005–2014, Atmospheric Chemistry and Physics, 15, 10 367–10 383,
     https://doi.org/10.5194/acp-15-10367-2015, 2015.

Manisalidis, I., Stavropoulou, E., Stavropoulos, A., and Bezirtzoglou, E.: Environmental and health impacts of air pollution: a review,
     Frontiers in Public Health, 8, 2020.

510 Marécal, V., Peuch, V.-H., Andersson, C., Andersson, S., Arteta, J., Beekmann, M., Benedictow, A., Bergström, R., Bessagnet, B., Cansado,
     A., et al.: A regional air quality forecasting system over Europe: the MACC-II daily ensemble production, Geoscientific Model Develop-
     ment, 8, 2777–2813, 2015.

Marinoni, A., Cristofanelli, P., Calzolari, F., Roccato, F., Bonafè, U., and Bonasoni, P.: Continuous measurements of aerosol physical param-
     eters at the Mt. Cimone GAW Station (2165 m asl, Italy), Science of the total environment, 391, 241–251, 2008.

515 MATLAB: R2022b Update 3, Tech. rep., The MathWorks Inc., 2022.

Mircea, M., Ciancarella, L., Briganti, G., Calori, G., Cappelletti, A., Cionni, I., Costa, M., Cremona, G., D'Isidoro, M., Finardi, S., et al.: As-
     sessment of the AMS-MINNI system capabilities to simulate air quality over Italy for the calendar year 2005, Atmospheric Environment,
     84, 178–188, 2014.

Murphy, A. H.: Skill scores based on the mean square error and their relationships to the correlation coefficient, Monthly Weather Review,
520      116, 2417–2424, 1988.

Ploton, P., Mortier, F., Réjou-Méchain, M., Barbier, N., Picard, N., Rossi, V., Dormann, C., Cornu, G., Viennois, G., Bayol, N., et al.: Spatial
     validation reveals poor predictive performance of large-scale ecological mapping models, Nature communications, 11, 4540, 2020.

Raftery, A. E., Gneiting, T., Balabdaoui, F., and Polakowski, M.: Using Bayesian model averaging to calibrate forecast ensembles, Monthly
     Weather Review, 133, 1155–1174, 2005.

525 Riccio, A., Barone, G., Chianese, E., and Giunta, G.: A hierarchical Bayesian approach to the spatio-temporal modeling of air quality data,
     Atmospheric Environment, 40, 554–566, 2006.

Rouil, L., Honore, C., Vautard, R., Beekmann, M., Bessagnet, B., Malherbe, L., Meleux, F., Dufour, A., Elichegaray, C., Flaud, J.-M., et al.:
     PREV'AIR: an operational forecasting and mapping system for air quality in Europe, Bulletin of the American Meteorological Society,
     90, 73–84, 2009.

530 Rue, H., Martino, S., and Chopin, N.: Approximate Bayesian inference for latent Gaussian models by using integrated nested Laplace
     approximations, Journal of the Royal Statistical Society: Series B (Statistical Methodology), 71, 319–392, 2009.

Sajani, S. Z., Miglio, R., Bonasoni, P., Cristofanelli, P., Marinoni, A., Sartini, C., Goldoni, C. A., De Girolamo, G., and Lauriola, P.: Saharan
     dust and daily mortality in Emilia-Romagna (Italy), Occupational and Environmental Medicine, 68, 446–451, 2011.

Scheuerer, M. and Möller, D.: Probabilistic wind speed forecasting on a grid based on ensemble model output statistics, The Annals of
535      Applied Statistics, 9, 1328–1349, 2015.

Schulzweida, U.: CDO user guide, Tech. rep., Max Planck Institute for Meteorology, 2022.

Shtein, A., Kloog, I., Schwartz, J., Silibello, C., Michelozzi, P., Gariazzo, C., Viegi, G., Forastiere, F., Karnieli, A., Just, A. C., et al.: Estimating daily $PM_{2.5}$ and $PM_{10}$ over Italy using an ensemble model, Environmental Science & Technology, 54, 120–128, 2019.

Singh, K. P., Gupta, S., and Rai, P.: Identifying pollution sources and predicting urban air quality using ensemble learning methods, Atmospheric Environment, 80, 426–437, 2013.

Stafoggia, M., Johansson, C., Glantz, P., Renzi, M., Shtein, A., de Hoogh, K., Kloog, I., Davoli, M., Michelozzi, P., and Bellander, T.: A random forest approach to estimate daily particulate matter, nitrogen dioxide, and ozone at fine spatial resolution in Sweden, Atmosphere, 11, 239, 2020.

Stortini, M., Arvani, B., and Deserti, M.: Operational forecast and daily assessment of the air quality in Italy: A Copernicus-CAMS downstream service, Atmosphere, 11, 447, 2020.

Taheri Shahraiyni, H. and Sodoudi, S.: Statistical modeling approaches for $PM_{10}$ prediction in urban areas; A review of 21st-century studies, Atmosphere, 7, 15, 2016.

Talagrand, O. and Vautard, R.: Evaluation of probabilistic prediction systems, in: Workshop Proceedings "Workshop on Predictability", ECMWF, Reading, UK, pp. 1–25, 1999.

Taylor, K. E.: Summarizing multiple aspects of model performance in a single diagram, Journal of Geophysical Research: Atmospheres, 106, 7183–7192, 2001.

Toth, Z., Talagrand, O., Candille, G., and Zhu, Y.: Probability and ensemble forecasts, in: Forecast verification: A practitioner's guide in atmospheric science, edited by Jolliffe, I. T. and Stephenson, D. B., chap. 7, pp. 137–163, John Wiley and Sons, First edn., 2003.

Vannitsem, S., Bremnes, J. B., Demaeyer, J., Evans, G. R., Flowerdew, J., Hemri, S., Lerch, S., Roberts, N., Theis, S., Atencia, A., et al.: Statistical postprocessing for weather forecasts: Review, challenges, and avenues in a big data world, Bulletin of the American Meteorological Society, 102, E681–E699, 2021.

Venables, W. N., Smith, D. M., and the R Core Team: An Introduction to R, Tech. rep., Max Planck Institute for Meteorology, 2022.

Whitaker, J. S. and Loughe, A. F.: The relationship between ensemble spread and ensemble mean skill, Monthly Weather Review, 126, 3292–3302, 1998.

WHO: WHO global air quality guidelines: particulate matter ($PM_{2.5}$ and $PM_{10}$), ozone, nitrogen dioxide, sulfur dioxide and carbon monoxide: executive summary, Tech. rep., World Health Organization, 2021.

Wilks, D. S.: Univariate Ensemble Postprocessing, in: Statistical Postprocessing of Ensemble Forecasts, edited by Vannitsem, S., Wilks, D. S., and Messner, J. W., pp. 49–89, Elsevier, 2018.

World Bank: The cost of air pollution: strengthening the economic case for action, https://openknowledge.worldbank.org/handle/10986/25013, 2016.

Xi, X., Wei, Z., Xiaoguang, R., Yijie, W., Xinxin, B., Wenjun, Y., and Jin, D.: A comprehensive evaluation of air pollution prediction improvement by a machine learning method, in: 2015 IEEE international conference on service operations and logistics, and informatics (SOLI), pp. 176–181, IEEE, 2015.

Zhang, H., Wang, Y., Hu, J., Ying, Q., and Hu, X.-M.: Relationships between meteorological parameters and criteria air pollutants in three megacities in China, Environmental Research, 140, 242–254, 2015.

Zhang, Y., Bocquet, M., Mallet, V., Seigneur, C., and Baklanov, A.: Real-time air quality forecasting, part I: History, techniques, and current status, Atmospheric Environment, 60, 632–655, 2012.

Zhou, L., Zhou, C., Yang, F., Che, L., Wang, B., and Sun, D.: Spatio-temporal evolution and the influencing factors of $PM_{2.5}$ in China between 2000 and 2015, Journal of Geographical Sciences, 29, 253–270, 2019.

**Table 2.** Statistics of the cross-validation study. RMSE is the root mean square error; CC is the correlation coefficient. Units of RMSE and bias are expressed in $\mu g/m^3$ for all pollutants.

| | | $PM_{10}$ | | | $PM_{2.5}$ | | | $NO_2$ | | | $O_3$ | | |
| --- | --- | --- | --- | --- | --- | --- | --- | --- | --- | --- | --- | --- | --- |
| | | CAMS data | stage 1 | stage 2 | CAMS data | stage 1 | stage 2 | CAMS data | stage 1 | stage 2 | CAMS data | stage 1 | stage 2 |
| RMSE | training | 12.32 | 9.99 | 5.13 | 8.80 | 8.22 | 4.06 | 28.43 | 22.34 | 13.02 | 21.62 | 16.18 | 7.42 |
| | validation | 12.21 | 10.82 | 7.96 | 7.91 | 7.71 | 5.74 | 26.59 | 24.36 | 19.02 | 19.97 | 16.51 | 13.99 |
| | prediction | 12.26 | 9.92 | 9.09 | 8.74 | 8.15 | 11.82 | 28.43 | 22.36 | 16.40 | 21.61 | 16.18 | 14.14 |
| Bias | training | -5.86 | 0.22 | -0.63 | -0.88 | 0.39 | -0.52 | -19.36 | 0.99 | -2.21 | 8.44 | 0.35 | -0.77 |
| | validation | -5.47 | 0.86 | -0.04 | 0.29 | 1.67 | -0.54 | -16.29 | 4.30 | 1.49 | 7.03 | -1.30 | -0.92 |
| | prediction | -5.86 | 0.20 | -0.97 | -0.87 | 0.37 | -0.58 | -19.35 | 0.98 | -2.35 | 8.43 | 0.37 | -1.54 |
| CC | training | 0.70 | 0.77 | 0.94 | 0.67 | 0.74 | 0.93 | 0.54 | 0.59 | 0.85 | 0.84 | 0.88 | 0.98 |
| | validation | 0.71 | 0.76 | 0.85 | 0.68 | 0.75 | 0.81 | 0.60 | 0.63 | 0.70 | 0.83 | 0.86 | 0.91 |
| | prediction | 0.70 | 0.77 | 0.79 | 0.67 | 0.74 | 0.53 | 0.54 | 0.59 | 0.75 | 0.84 | 0.88 | 0.92 |

**Table 3.** Average width for the 50% probability interval around the predicted value for the estimation dataset (first row), validation dataset (second row) and in prediction mode (third row). Units are expressed in $\mu g/m^3$ for all pollutants.

| | $PM_{10}$ | | | $PM_{2.5}$ | | | $NO_2$ | | | $O_3$ | | |
| --- | --- | --- | --- | --- | --- | --- | --- | --- | --- | --- | --- | --- |
| | CAMS data | stage 1 | stage 2 | CAMS data | stage 1 | stage 2 | CAMS data | stage 1 | stage 2 | CAMS data | stage 1 | stage 2 |
| estimation | 8.3 | 11.1 | 3.3 | 5.9 | 8.1 | 2.5 | 19.2 | 25.7 | 7.5 | 14.6 | 23.4 | 7.9 |
| validation | 8.2 | 11.5 | 4.4 | 5.3 | 7.8 | 3.3 | 17.9 | 26.3 | 10.8 | 13.5 | 23.5 | 15.1 |
| prediction | 8.3 | 11.1 | 7.1 | 5.9 | 8.1 | 5.1 | 19.2 | 26.0 | 10.5 | 14.6 | 23.5 | 14.4 |